**Wind and Structures**, *Vol. 18, No. 5 (2014) 529-548*
DOI: http://dx.doi.org/10.12989/was.2014.18.5.529 

# Numerical calculations of aerodynamic performance for ATM train at crosswind conditions

Mohammad Ali Rezvani* and Masoud Mohebbi[a]

*School of Railway Engineering, Iran University of Science and Technology, Tehran, Iran, 16846-13114*

*(Received January 19, 2013, Revised July 26, 2013, Accepted February 14, 2014)*

**Abstract.** This article presents the unsteady aerodynamic performance of crosswind stability obtained numerically for the ATM train. Results of numerical investigations of airflow past a train under different yawing conditions are summarized. Variations of occurrence flow angle from parallel to normal with respect to the direction of forward train motion resulted in the development of different flow patterns. The numerical simulation addresses the ability to resolve the flow field around the train subjected to relatively large yaw angles with three-dimensional Reynolds-averaged Navier-Stokes equations (RANS). κ-ε turbulence model solved on a multi-block structured grid using a finite volume method. The massively separated flow for the higher yaw angles on the leeward side of the train justifies the use of RANS, where the results show good agreement with verification results. A method of solution is presented that can predict all aerodynamic coefficients and the wind characteristic curve at variety of angles at different speed.

**Keywords:** high speed train; aerodynamic performance; crosswind condition; numerical simulation

## 1. Introduction

Although the first accidents of trains due to strong crosswinds date back to the 19th century, it is in recent years that the effects of crosswinds attracted considerable attention. Recent developments in railway transportation have shown the trend for faster, more comfortable and more energy efficient trains. In order to achieve the maximum performance and cost efficiency, it is necessary to build ever lighter trains. Unfortunately, decrease in weight negatively mutates the crosswind stability. Therefore, crosswind stability of trains is an important topic in this industry. There is no definitive solution for it, yet.

Many researchers including Cheli *et al*. (2010), Diedrichs (2005), Baker *et al*. (2004), Suzuki *et al*. (2003), Baker (2008) analyzed the problem that involves both rolling stock and high speed trains. Cheli *et al*. (2012) studied the crosswind action on rail vehicles. They evaluated the aerodynamic performance of a train in terms of safety toward the crosswind and defined the characteristic wind curves. Yau (2011) presented a framework of nonlinear dynamic analysis of a low-speed moving magnetically levitated vehicle subjected to crosswinds and controlled using a

*Corresponding author, Assistant Professor, E-mail: rezvani_ma@iust.ac.ir
[a] Ph.D. Student, E-mail: masoudmohebbi.iust@gmail.com


http://www.techno-press.org/?journal=was&subpage=8 ISSN: 1226-6116 (Print), 1598-6225 (Online)

clipped-LQR actuator with time delay compression. Xu and Guo (2003), investigated the dynamic behavior of high-sided road vehicles subjected to sudden crosswind gust. Sharma *et al*. (2008) exercised a number of passive aerodynamic drag reduction methods separately and then in combination on an intercity bus model. Cheli *et al*. (2006), discussed a numerical and experimental procedure to improve EMUV250 train aerodynamic performance under crosswind conditions. They evaluated the effects of different parts of the train geometry in defining the aerodynamic forces and in particular offered characteristic wind curve that limits wind speed for the safety of the train and avoid the risk of overturning. Hemida and Kraajnvic (2006), modeled overall flow structure around a high speed train at crosswinds using LES. Their calculations were for both 35 and 90 degrees yaw angles. Crosswind flow mainly shows transient eddy at 90 degree yaw angle, while crosswind flow at smaller yaw angle is like a slender body train. Hemida *et al*. (2005), while studying the flow around a simplified model of high speed train under cross wind suggested that separation bubbles appear in the middle of ceiling plate. Axial flow arising in the lateral edge near the nose of the train led to the creation of two strong vortices in a sequence that starts at the nose of the train. Hemida and Baker (2010), in LES simulation of flow around a freight train subjected to crosswind at a 90 degree yaw angle realized that flow fields around the freight cars are very complex compared to the passenger cars. Numerical studies of Masson *et. al*. (2009), revealed that the improved geometry of the floor of the train has a key role in improving the aerodynamic coefficients. Diedrichs (2003) studied the lateral stability of ICE2 high speed train in the range of 12.2 to 40 degree yaw angles. The main results were a collection of independent aerodynamic coefficients for the first and the last rail cars in the train makeup. Also, Diedrichs (2009) modeled ICE2 train stability against crosswind for small yaw angles. He studied instability effects of aerodynamic loads using DES method for the control unit of ICE2 high speed train. Yang *et al*. (2007), studied the effects of a truck passing a stationary car with the hood of the car open. They found that some critical parameters were lateral distance between the stationary cars and the passing truck, the angle of the open hood and the speed of the truck. Masbernat *et al*. (1993) exhibited 3D computations of the flow field around the French high speed train (TGV). The Reynolds averaged compressible Navier-Stokes equations discretised on an unstructured grid using the finite element method.

It is the objective of this article to present the results of a numerical investigation of crosswinds on aerodynamic train model (ATM). It is aimed at exploring the predictive accuracy of the flow fields and all the interesting aerodynamic features of a high speed train. The numerical work confines attention to different yaw angles.

Calculations are compared to experimental finding obtained by Rocchi *et al*. (2009) performed in the two sections of the Politecnico di Milano wind tunnel (PMWT) and at the wind tunnel T103 of the Central Aerodynamic Institute TsAGI (TsAGI) on the same model train. The main objective is to verify the calculations regarding the aerodynamic loads and part of the static pressure distribution around the car body. To this end, the Reynolds number (Re) and geometry of the experiments concerning the vehicles and wind tunnel are similar to those of the calculations.

Two different equations for turbulent closure methods are checked and it is found that the best agreement with experimental results corresponds to the κ-ε realizable model. All the results presented in this paper are obtained with this model.

The added contribution of this research is in the method of solution that can predict all aerodynamic coefficients and the wind characteristic curve at variety of angles at different speed. To the knowledge of the authors no such comprehensive results are available in the corresponding

literature. All other reported results are limited to some wind tunnel test results and/or limited by a limited domain of speed and angels.

## 2. The theoretical background

In external flow of fluids around bodies, changes in pressure and velocity fields occur. When designing and constructing bodies exposed to external flows it is of great importance to take the characteristic of the flow, i.e., pressure distributions and velocity fields that arise, in consideration.

The differential approach in analysis of fluid flow is based on a number of governing equations which describe the flow in different aspects. These equations are mathematical statements of the conservation laws of physics. The laws of conservation yields that mass, momentum (according to Newton's second law) and energy (according to the first law of thermodynamics) must be conserved (Versteeg and Malalasekera 2007). The Navier-Stokes equations are derived from the previously mentioned laws. They are applied to an infinitesimal control volume. The equations are valid for incompressible flow with constant viscosity for a Newtonian fluid; a fluid where the viscous shear stresses are proportional to the velocity gradient of the deformation. A rule of thumb yields that the flow can be considered incompressible for $Ma \leq 0.3$ where $Ma$ is the mach number of the fluid. In ambient conditions this yields incompressibility for velocities below approximately 100 m/s. Also the assumption of constant viscosity is true in the case of small pressure gradients. The resulting equations are second-order nonlinear partial differential equations (PDE) describing the behavior of fluids. The equations are relating pressure (p), density (ρ) and viscosity (μ) of the fluid to each other, (White 2008).

Computing the flow is becoming more and more efficient with increasing computer power and the Navier-Stokes equations make the foundation for these calculations.

### *2.1 Definitions of the aerodynamic loads*

When a train cruises in a side wind it experiences aerodynamic forces and momentums. The aerodynamic forces include the drag force, the side force and the lift force. The drag force opposes the forward motion of the vehicle. The side force pushes the vehicle to the side. The lift force acts upward while intending to raise the vehicle up from the ground. The moments corresponding to these forces include the rolling, the yawing and the pitching moments, respectively. The principal aerodynamic loads in terms of forces and moments with respect to the direction of (x,y,z) are defined according to EN standard (prEN 14067-6). According to EN 14067-1 the non-dimensional aerodynamic coefficients are expressed as follows,

Forces

$$(F_d, F_s, F_l) = \mathrm{q}.\mathrm{A}_t\,(C_d, C_s, C_l) \tag{1}$$

Momentums

$$(M_\gamma, M_p, M_y) = \mathrm{q}.\mathrm{A}_t.\mathrm{l}_t\,(C_\gamma, C_p, C_y) \tag{2}$$

Dynamic Pressure

$$q = \frac{\rho U_{\infty}^{2}}{2} \tag{3}$$

Pressure

$$p - p_{\infty} = q.C_{p} \tag{4}$$

$p$ is the local static pressure, $U_{\infty}$ is the free stream velocity and $p_{\infty}$ is the free stream static pressure, $A_t$ is the train surface area and $l_t$ is the length of the train.

In Fig. 1 the flow situation is defined with relative wind speed of $U_R$ and yaw angle $\beta$. The origin of the coordinate system is placed in the middle part of the body, at the centerline of the vehicle at the top of the rail. The x,y,z point in the directions of the train, perpendicular to the train side and vertically toward the ground, respectively. In Fig. 1 $h_t$ is the vehicle height. The loads and static pressure ($C_p$) are scaled with the dynamic pressure based on $U_R$.

The geometrical scaling of the aerodynamic loads is at full scale dimension (i.e., $l_t$=3 m and $A_t$=10 m$^2$).

The roll moment of Eq. (2) can be supplemented with a more important variable related to overturning, namely the rolling moment about the lee-rail, expressed in Eq. (5)

$$C_{R-LR} = C_{Roll} + C_{Lift}(b_0 w_t / 2h_t^2) \tag{5}$$

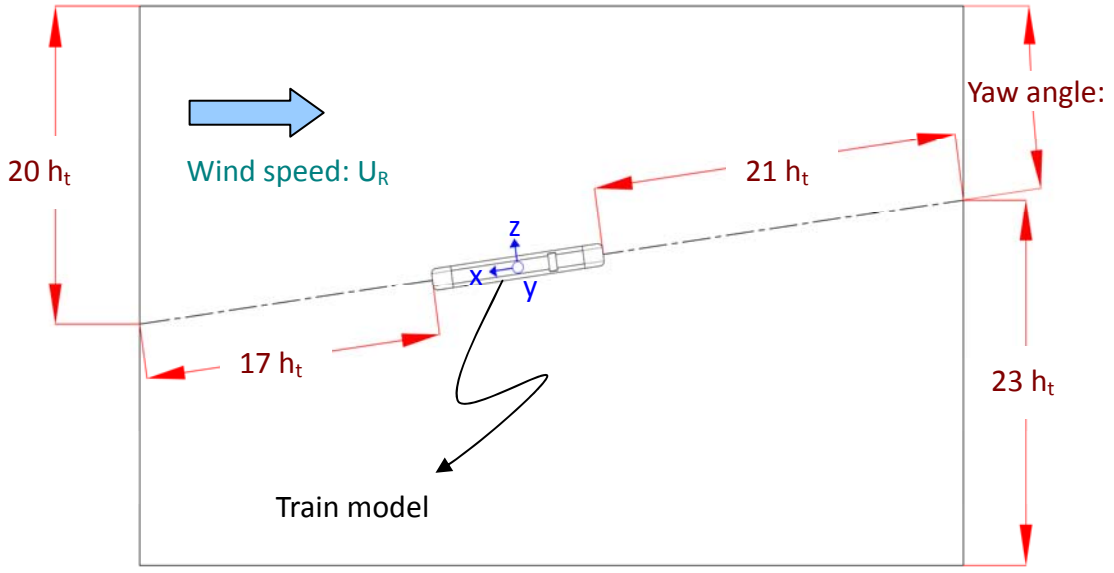


Fig. 1 The top view of the computational domain

The parameter $2b_o=1.5$ m, represents the nominal lateral distance between the contact points of a wheelset for a standard gauge track. $W_t$ is the train width and $h_t$ is the train height. The $C_{R\text{-}LR}$ predicts vehicle overturning in a two dimensional sense.

It order to justify the selected domain that is presented in Fig. 1 (i.e., equivalent to that of experimental test), it needs to be reminded that the idea is to minimize the sources of any discrepancy between the numerical and experimental results. Such calculation domain, compared with the wind tunnel test can provide more accurate results. In reality, the space surrounding a moving train is unlimited in all directions and the rail is the only limiting surface. While in wind tunnel test, the proximity of the flow boundaries to the vehicle causes deformation of the flow around the vehicle. Such flow deformation affects the flow angle, distribution of the speed and pressure around the vehicle and the shear stress on the vehicle surfaces turn to be different. As a result the forces and moments applied on the vehicle change. In the wind tunnel the solid walls prevent development of the fluid flow around the test specimen and make it different compared with the test at open air. Therefore, the velocity vectors around the test specimen tend to be larger than the real case scenario that happens in open air.

Wind tunnel tests naturally have limitations on the maximum speed of flow and speed variations. The physical domain of the calculations must be large enough in order to prevent the errors rising from the boundaries. Axelssson *et al*. (1998) while studying a passenger coach showed that improper distance can create incorrect pressure domain around the train. Kheir *et al*. (2000) and Rolen *et al*. (2004) used simple models containing two vehicles. Kheir used a domain at a scale of 20:10:10 (front: side: back) of the train height. The extended domain selected by Rollen was 19:9:5.

## 3. The vehicle model

The vehicle model is a 1:10 simplified scaled version of an ICE2 train. That is the so called Aerodynamic Train Model (ATM). It consists of 2 cars, 1 inter-car gap and simplified bogies. The height $h_t$, width $w_t$, and length $l_t$ of the model are 0.385 m, 0.299 m and 3.557 m, respectively. These are the dimensions of the model also used by Rocchi *et al*. (2009). The justification for using this model is in the fact that the purpose of the present article is to establish a numerical method that can predict the wind tunnel test results, with the acceptable degree of accuracy.

## 4. The computational fluid dynamic

Computational Fluid Dynamics, usually and from here on abbreviated to CFD, is a numerical method to compute the dynamics of a fluid. In brief, it is implemented by dividing a computational domain into small cells where the flow is modeled and flow equations are solved.

CFD simulations have been executed to investigate the flow field around the train and the pressure distribution on the train surfaces in order to understand the train aerodynamics in terms of reaction to the transversal wind. As a matter of fact, CFD simulations have the potential to model real situations better than wind tunnel tests and with fewer attempts. A number of assumptions, simplifications and hardships refer to both wings of investigation. Usually the time and length scales of the wind and the topography of the surroundings adjacent to the track are neglected (Gawthrope 1994). The majority of flow cases studied herein is computed with the commercially

available flow simulation software ANSYS Fluent (2012). The investigation of flow field around the ATM train model at different wind exposure carried out by means of 3D CFD analysis. The simulation results are validated by a comparison between experimental findings in terms of the global forces and moments.

Since almost all fluid flows are turbulent, different methods are used in order to simulate turbulence. These can be divided in different categories where some of them are; Turbulence models for Reynolds-Averaged Navier-Stokes (RANS) equations, Large Eddy Simulation (LES), Direct Numerical Simulation (DNS) and Lattice Boltzmann Method (LBM).

The LBM differs from the other methods by simulating the movements of particles and aims at recovering the hydrodynamics of the Navier-Stokes equation. RANS on the other hand, uses the Navier Stokes equations as a starting point and aims at solving them (Kandasamy *et al.* 2002). DNS does not use a turbulence model; it computes all the turbulent velocity fluctuations and therefore demands both small time steps and cells that require substantial computer resources. LES focuses on the large eddies in the flow and requires quite large computer resources. However, the most common way to simulate turbulence is to calculate the time averaged properties of the flow, such as the mean pressure, mean velocity and so on, which in most cases give sufficient information about the flow. This method has a modest computer demand and is conducted with RANS-models (Versteeg and Malalasekera 2007).

### *4.1 Turbulence models for the Reynolds-Averaged Navier-Stokes equations*

There are several different turbulence models within the RANS method that in different ways model the extra terms that forms when the Navier-Stokes equations are time-averaged. Some models worth mentioning are the mixing length model, the κ-ε model, the κ-ω model and the Reynolds stress model, which have none, two, two, and seven additional transport equations, respectively. These equations need to be solved in addition to the RANS equations (Versteeg and Malalasekera 2007). Naturally, all models have their advantages and disadvantages. The Mixing length model is not suitable for flow with separation and circulations, and the Reynolds stress model is the most complex one of these four and needs fairly large computer capability. There are also two-equation models κ-ε and κ-ω the so-called Eddy viscosity models, which means that they are based on the turbulent viscosity. In the κ-ε model the two transport equations are solved for the turbulent kinetic energy κ and its dissipation ε . ω is the dissipation rate per unit turbulence kinetic energy, in other word the specific dissipation rate $\omega \approx \varepsilon / \kappa$. One of the major differences between these two models is that the standard κ-ε model needs wall functions to resolve the boundary layer, whereas the κ-ω model is feasible to use all the way into the wall. The κ-ω model on the other hand, deals with problems when it comes to the initial value of ω in the free stream, the results seem to depend on this value. Therefore, in order to properly depict the flow field and consequently the wall-stress on the train surface, a κ-ε realizable turbulence model with non-wall functions treatment is adopted for this project since it is widely used in vehicle aerodynamics and is efficient and accurate.

### *4.2 The fluid flow assumptions*

In Fig. 1 dimensions of the computational domain are drawn. It consists of a rectangular box with height $7.5h_t$. To avoid the pressure at the inlet to the boundary, to interfere with the vehicle,

and to provide a sufficiently long wake region, the bounding box is extended before and after the $17h_t$ and $21h_t$, respectively. No-slip conditions are applied on the extensions. Here, follows a summary of all boundary conditions:

1) Low turbulence block profile inlet condition for $U_R$ which corresponds to Reynolds number of $0.7\times10^6$ to $2.5\times10^6$ based on train height.
2) No-slip standard logarithmic law of the wall boundaries used for the surfaces of the train and ground.
3) Ceiling and outer ground use symmetrical boundary and slip conditions, respectively.
4) The south boundary is the outlet based on the fixed pressure.

The boundary conditions are selected on the basis that can provide the real scenarios as much as possible. It is to form the turbulent flow and to put the train model under the layer of the logarithmic law that represents the completely developed flow.

In order to simulate the experimental boundary conditions slip conditions for surfaces of the side walls and the roof of the vehicle are considered.

The fourth boundary condition is to allow for extensions of the flow (wake and slip stream). Such conditions normally observed under real conditions but cannot be completely formed under wind tunnel situations. This is due to the limitations and the small sizes of the boundaries in wind tunnel.

In the numerical procedure a multi-block mesh is used in order to be able to establish minor geometrical or mesh modifications without having to mesh the whole model again. In this work the tetrahedral cell meshing technique is adopted with a finer spatial resolution close to the train surface in order to properly reproduce the geometrical details and to better approximate the higher gradients in this zone.

Near the vehicle side walls, the grid refined to acquire a unit wall distance for the first grid point $y^+=yu^*/v<100$, where $u^*$ is the friction velocity and ν is the kinematic viscosity, $1.4\times10^{-5}$ $m^2/s$, as in Fig. 2.

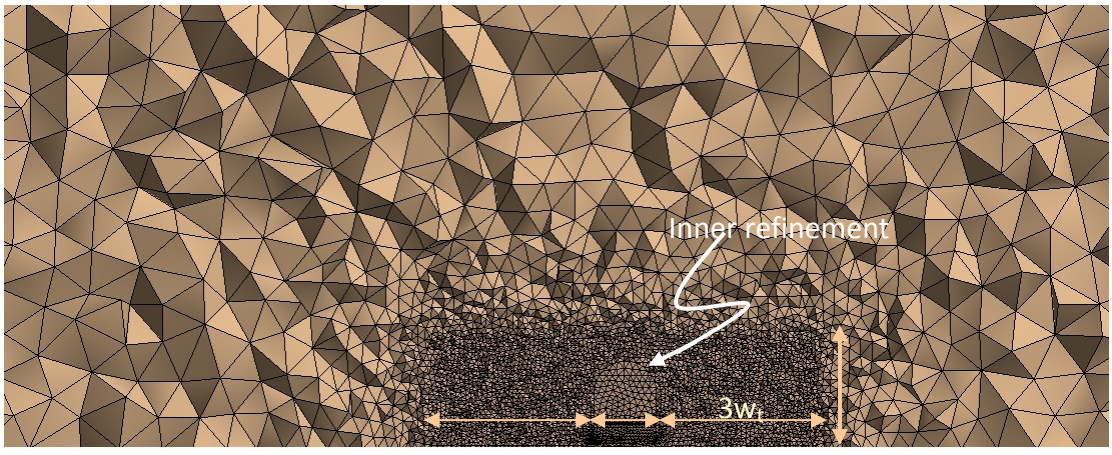


Fig. 2 Tetrahedral meshes with a finer spatial resolution close to the train surface

The mesh in the train region created requiring a first cell height equal to 1mm, corresponding to a $y^+$ of about 35 for simulated cases. This value recommended use of standard wall functions ($30 < y^+ < 300$). The cell count is from $7.2\times10^6$ to $18.5\times10^6$ due to inner viscous part of the boundary layer adjacent to the vehicle, (Fig. 2). A second order upwind method was chosen for the Navier-Stokes equations while the velocity-pressure coupling is performed with a coupled scheme.

### *4.3 The mechanical interpretation of the stability against crosswind*

It is already stated that a major aim of this article is the prediction of the stability of a rail vehicle against the crosswinds. In order to satisfy the key task, it should be possible to calculate the distribution of the lateral and lifting forces, and then the exact position of the centre of gravity of the vehicle. It is then possible to convert all loads into the overturning momentum about the lee-rail (Eq. (5)). Hence the identification of the most plausible point in overturning the vehicle is justified. The Group Standard 2000 (GS2000) developed a method for predicting the speed of wind that is capable of overturning a rail vehicle along a straight ideal track. It is calculated from the equivalent momentum about the lee-rail. By using the common definitions for the forces from the aerodynamic loads, the equivalent momentum is calculated as

$$M_{Grav} = m.g.b_0 - G_0 = M_{Aero} = \frac{1}{2}\rho.h_t^2.l_t.C_{R-LR}(U_t).U_R^2 \tag{6}$$

where $M_{Grav}$ and $M_{Aero}$ are the overturning and unstable gravity and aerodynamic momentums about the lee-rail. $G_0$ is the rolling momentum that causes displacement of the rolling and lateral suspension system under wind loading under any asymmetric mass of the assembled vehicle. However, $G_0$ is sometimes deleted for simplicity. By replacing the resultant wind $U_R^2$ with $U_t^2+U_w^2$ the velocity of the main wind is calculated as following

$$U_w = \sqrt{\frac{2.m.g.b_0}{\rho.h_t^2.l_t.C_{R-LR}(U_t)} - U_t^2} \tag{7}$$

GS2000 recommended that such aerodynamic coefficients be used for variety of wind stream angles for the test vehicle. It depends only on the vehicle speed of travel. The aerodynamic coefficients are obtained based on $C_{R\text{-}LR}(U_t)$ in Eq. (5).

However, there are more general equations that do not include the dynamic effects but consider the condition of deflection on the inclined bed according to Fig. 3 (Baker 1991). In what continues by estimating the condition of overturning the following assumptions are available

$$\begin{aligned} &\cos\theta_c \approx 1, \\ &\theta_c \approx \sin\theta_c = \frac{h_c}{2b_0} \end{aligned} \tag{8}$$

The equivalent momentum about the lee-rail can then be obtained based on the train speed $U_t$ that causes 100% unloading of the wheel as a function of the deviation angle $\beta$ (as a sole unspecified parameter).

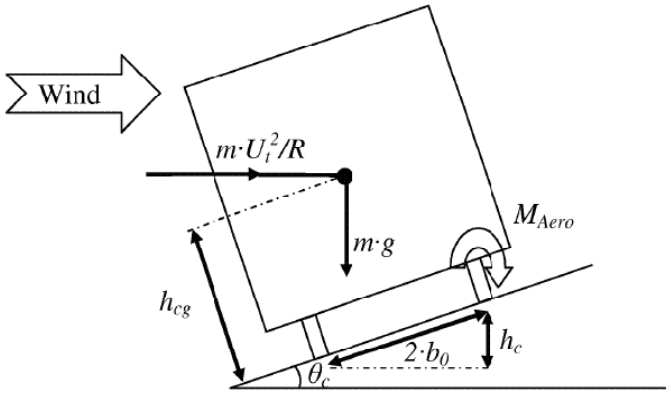


Fig. 3 The schematic of overturning of a rail vehicle

$$U_t \tan(\beta) - \sqrt{\frac{2.m.g}{\rho.h_t^2.l_t.C_{R-LR}(\beta)}\left[b_0 + \frac{h_{cg}.h_c}{2b_0} + \frac{U_t^2}{R.g}\left(\frac{h_c}{2} - h_{cg}\right)\right] - U_t^2} = 0 \tag{9}$$

The coefficient of rolling momentum $C_{R\text{-}LR}(U_t)$ is replaced with $C_{R\text{-}LR}(\beta)$ with $\beta=arctan(U_w/U_t)$. $U_w$ is perpendicular to $U_t$.

Such a method is used as an effective criterion in designing the new tracks for providing stability against lateral winds.

## 5. The results and discussions

### *5.1 The flow structure*

A train exposed to crosswind produces a flow that in some sense is similar to that around an aircraft wing, Fig. 4.

The nose region is subjected to the largest pressures, which arises from the suction pressure ($P_{1\text{-}}$) on the leeward side. In addition, a high pressure ($P_{2+}$) is produced about the stagnation region, which is limited to the dynamic pressure. When the flow curves around the top leeward corner of the nose it generates a fairly stationary lee vortex. Further down the cross section, where the roof tapering starts, an additional suction pressure ($P_{3\text{-}}$) is generated along the top windward corner.

### *5.2 The aerodynamic coefficients*

Figs. 5(a)-5(f) present variation of the aerodynamic coefficients with yaw angle at various speeds. The results are compared and validated with the experimental data from Rocchi *et al*. (2009). The experimental data refer to the PMWT wind tunnel.

Drag, lift and side forces specific to each side were obtained from the calculation. In order to make them more efficient compared to previous studies and the future, these numbers are provided in the form of dimensionless coefficients. In Fig. 5(a) the drag coefficient increases with increasing

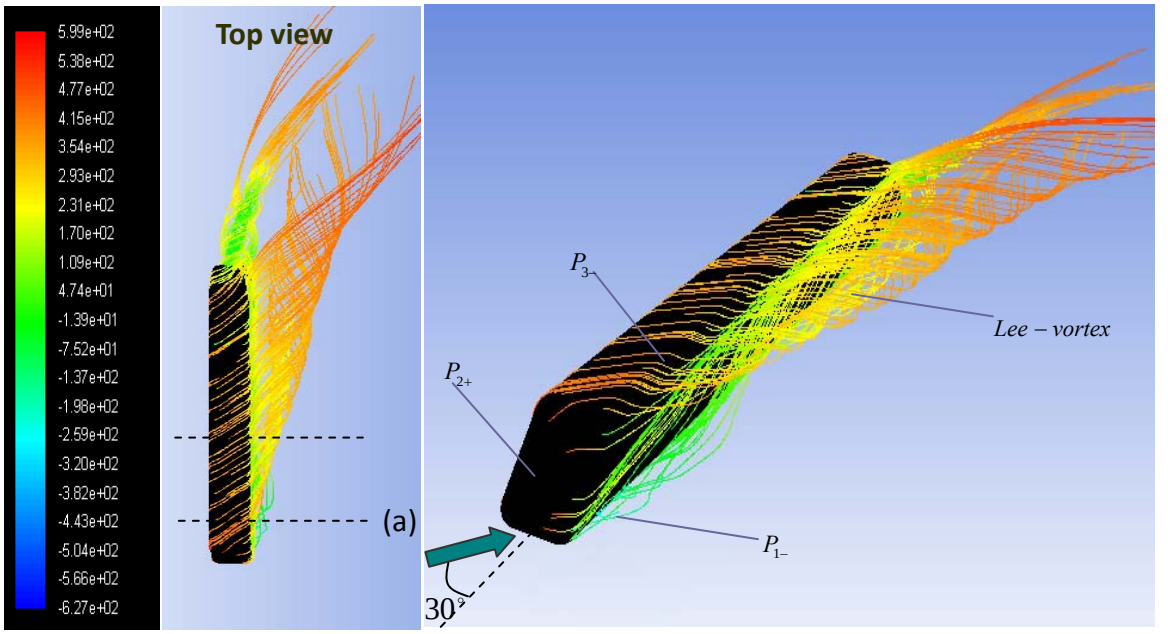


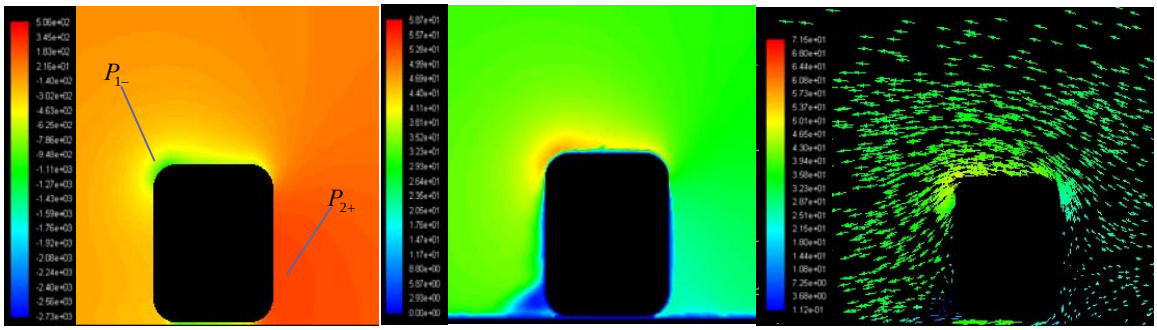


(a)

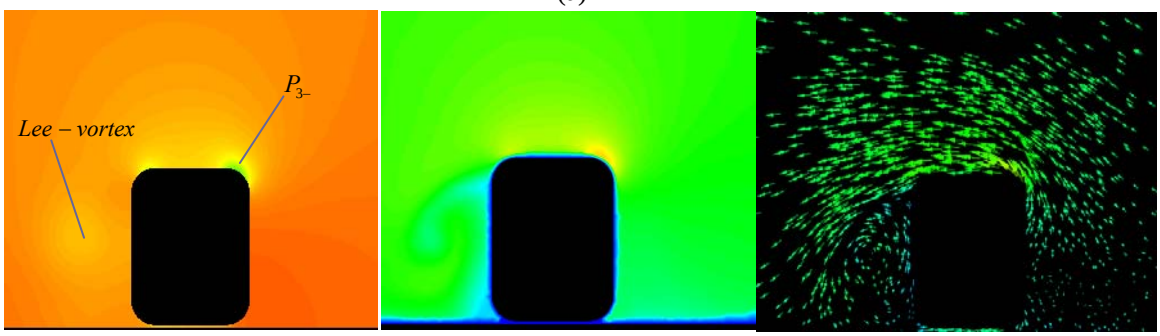


(b)

Fig. 4 Illustration of surface pressure, lee side vortex and velocity field for the ATM train at (a) *x/l=0.1* and (b) *x/l=0.4* from the nose

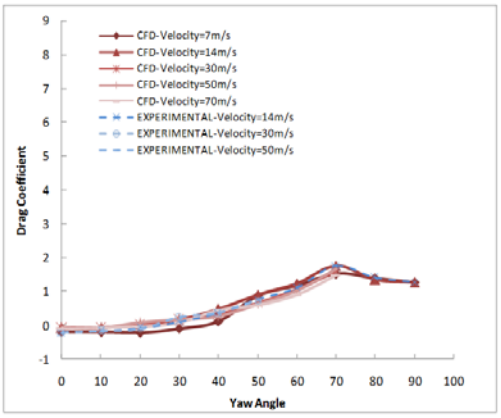


(a) Drag Coefficient

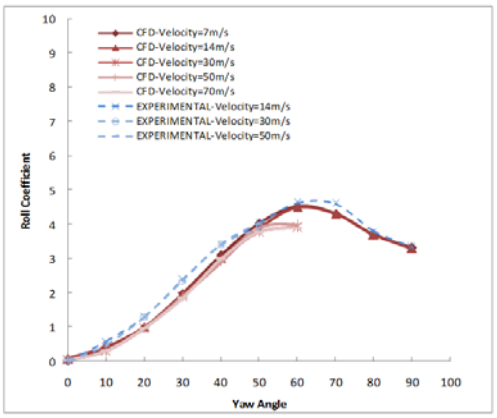


(d) Rolling Moment Coefficient

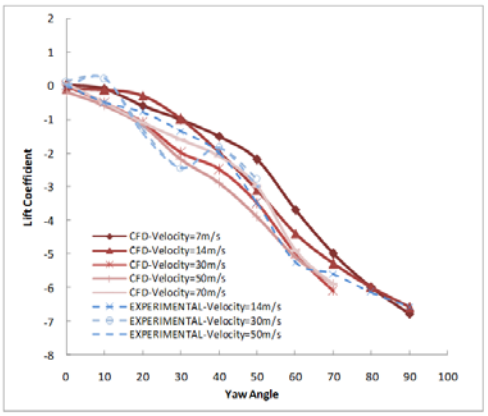


(b) Lift Coefficient

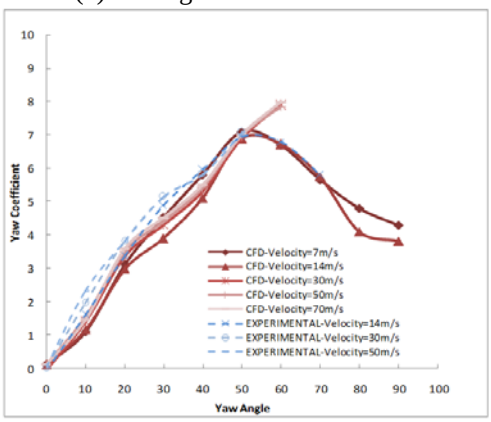


(e) Yawing Moment Coefficient

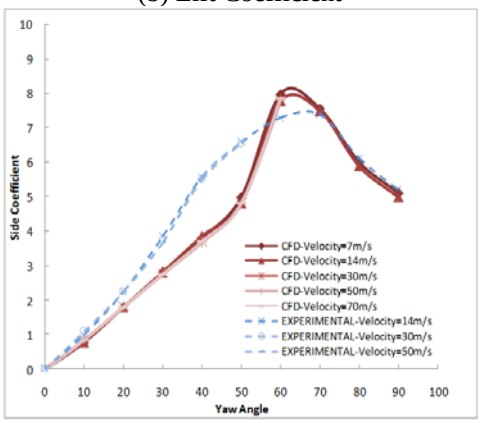


(c) Side Coefficient

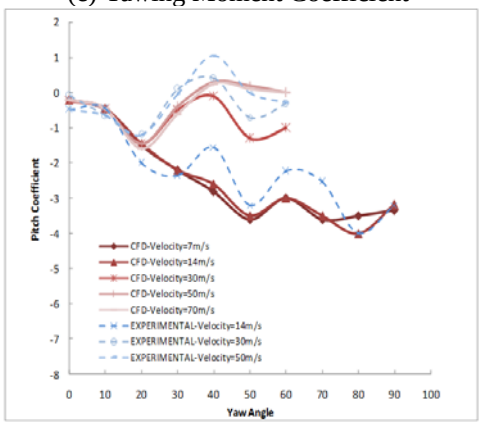


(f) Pitching Moment Coefficient

Fig. 5 Variation of the aerodynamic coefficients with yaw angles from 0 to 90 degrees at various speed from 7 to 70 m/s

yaw angle. This increase has continued to 70 degrees and then with increasing yaw angle, reduced coefficient is observed. Also, it was found that increasing the wind speed has no noticeable effect on the drag coefficient while it was expected of the train aerodynamic nose. Fig. 5(b) shows a little force for the yaw angle limited to 10 degrees with lift force coefficient. For higher angles, more growth and sharply increased volatility. A little dependency is observed for higher angles. Fig. 5(c) shows increased side force with increasing yaw angle and the symmetric behavior for angles greater than 50 degrees. The side force coefficient is not dependent on the wind speed.

Rolling moment is the most important parameter shown in Fig. 5(d). Rolling moment is responsible for the loading and unloading of wheelsets. Rolling moment increases with increasing yaw angle and the asymmetric behavior is observed for angles of about 50 degrees. Rolling moment does not change with increasing wind speed. The yawing moment is shown in Fig. 5(e). Yawing moment was increased monotonically with increasing yaw angle and small dependency with the wind speed. The yawing moment affects the load distribution between leeward and windward sides. Pitching moment is shown in Fig. 5(f).

This is the coefficient that is more sensitive to the wind speed variations compared to the rest of the aerodynamic coefficients. However, amounts are relatively small and have little effect on the aerodynamic performance of overturning.

Coefficient of rolling momentum about lee rail is shown in Fig. 6. This coefficient increases with increasing yaw angle to 60 degrees, and dramatically reduces in high wind speeds.

In Table 1 a comparison between the numerical and experimental aerodynamic coefficients in $\beta=30^o$ and $U_R$=30 m/s is listed. It is possible to expand Table 1 in order to cover a variety of angles and velocities. However, the results that are presented in Figs. 5(a)-5(f) include all such data. All discrepancies between the numerical and experimental results for the sample case are also presented in Table 1.

At this stage, the differences between the numerical and experimental data need to be highlighted. There are differences up to 27%-30% for Cfy and Cfz at 30$^o$ and higher differences at other angles (up to approximately 50% for Cfy).

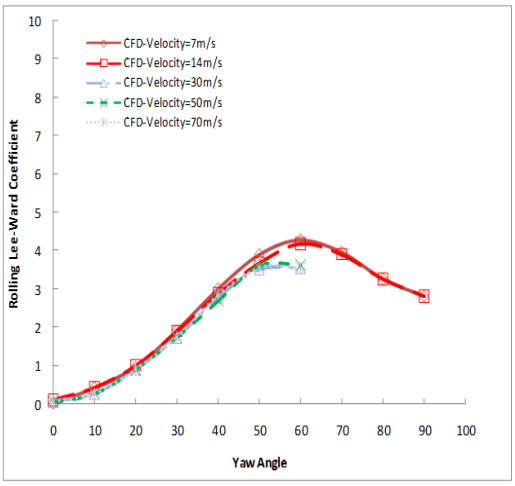


Fig. 6 Roll moment about the lee-rail with yaw angles at various speed

The sources of the so called discrepancies include the differences in the methodology of solution, the degree of accuracy in the numerical models, accuracy in taking the measurements, errors due to simplifications, etc. Also deviation percentage is obtained according to Eq. (10)

$$Deviation = 1 - \frac{C_{CFD}}{C_{Wind\ tunnel}} \tag{10}$$

Table 1 Aerodynamic coefficients for ATM train and the corresponding deviation percentages

| | Velocity (m/s) | 7 | 14 | 30 | 50 |
|---|---|---|---|---|---|
| $C_{Drag}$ | Numerical Simulation | -0.111 | 0.14 | 0.18 | 0.16 |
| | Wind Tunnel | 0.00 | 0.11 | 0.21 | 0.20 |
| | Deviation Percentage | - | -27% | 14% | 20% |
| $C_{Lift}$ | Numerical Simulation | -1.10 | -1.02 | -2.02 | -2.22 |
| | Wind Tunnel | -1.50 | -1.35 | -2.40 | -2.43 |
| | Deviation Percentage | 27% | 24% | 16% | 9% |
| $C_{Side}$ | Numerical Simulation | 3.90 | 2.90 | 2.80 | 2.90 |
| | Wind Tunnel | 5.56 | 3.70 | 3.62 | 3.61 |
| | Deviation Percentage | 30% | 22% | 23% | 20% |
| $C_{Rolling}$ | Numerical Simulation | 3.20 | 2.01 | 1.95 | 1.96 |
| | Wind Tunnel | 3.49 | 2.32 | 2.25 | 2.29 |
| | Deviation Percentage | 8% | 13% | 13% | 14% |
| $C_{Yawing}$ | Numerical Simulation | 5.89 | 3.94 | 4.39 | 4.38 |
| | Wind Tunnel | 6.41 | 4.87 | 5.11 | 5.12 |
| | Deviation Percentage | 8% | 19% | 14% | 14% |
| $C_{Pitching}$ | Numerical Simulation | -2.78 | -2.18 | -0.50 | -0.40 |
| | Wind Tunnel | -2.19 | -2.32 | 0.00 | 0.00 |
| | Deviation Percentage | -27% | 6% | - | - |

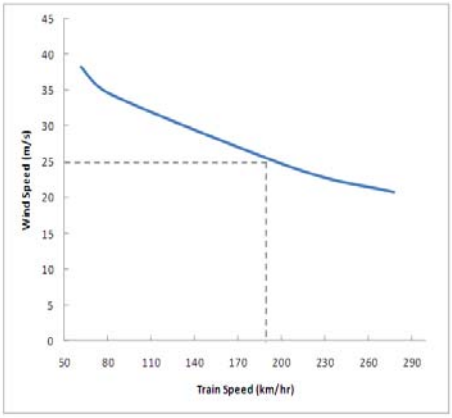


Fig. 7 The calculated train speed limit with the wind flow

With rolling moment coefficient about the lee rail and the minimum possible weight one can calculate the maximum allowable speed for each wind speed to prevent overturning.

The train speed limit due to the wind is shown in Fig. 7.

It is observed that the probability for train stability at higher speed is greater if a dynamic head pressure increases slowly with the train speed compared with increasing the rolling moment coefficient. For example at the wind speed of 25 m/s, the maximum permissible speed of the train to prevent overturning should not exceed 190 km/h.

### *5.3 The pressure distribution*

Fig. 8 gives the comparison of the pressure distribution for the train for both windward and leeward sides. As expected, the pressure decreases with the yaw angle for leeward side and increases for windward side. This leads to the formation of flow separation behind the train.

It makes sense to compare the numerical and the experimental results in terms of pressure distribution in order to better understand the differences found in the corresponding force/moment coefficients. The results for the pressure distribution are presented in Figs. 4 and 8. Such comparisons can be made by the data provided in these figures. Further processing of data are omitted in order to save some space. Fig. 9 demonstrates the time averaged of the aerodynamics in terms of the velocity magnitude at $z/h_t=0.2$ for different yaw angles ranging from 0 to 90 degrees. Fig. 10 presents the total pressure distribution on a section of the train model for yaw angles from 0 to 90 degrees. The computational challenges involve the influencing flow on the windward side, the wake flow on the leeward side, the twisted flow along the train surfaces, separation lines along different parts, growth of boundary layers, and prognostication of a properly flow separated beneath and above the vehicles.

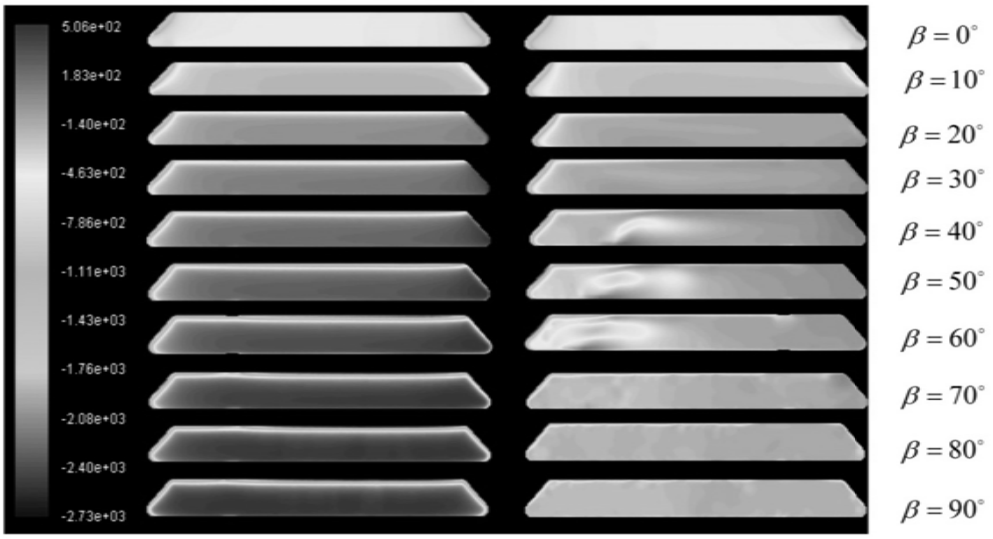


Fig. 8 Pressure distribution for the leeward (right) and windward (left) sides

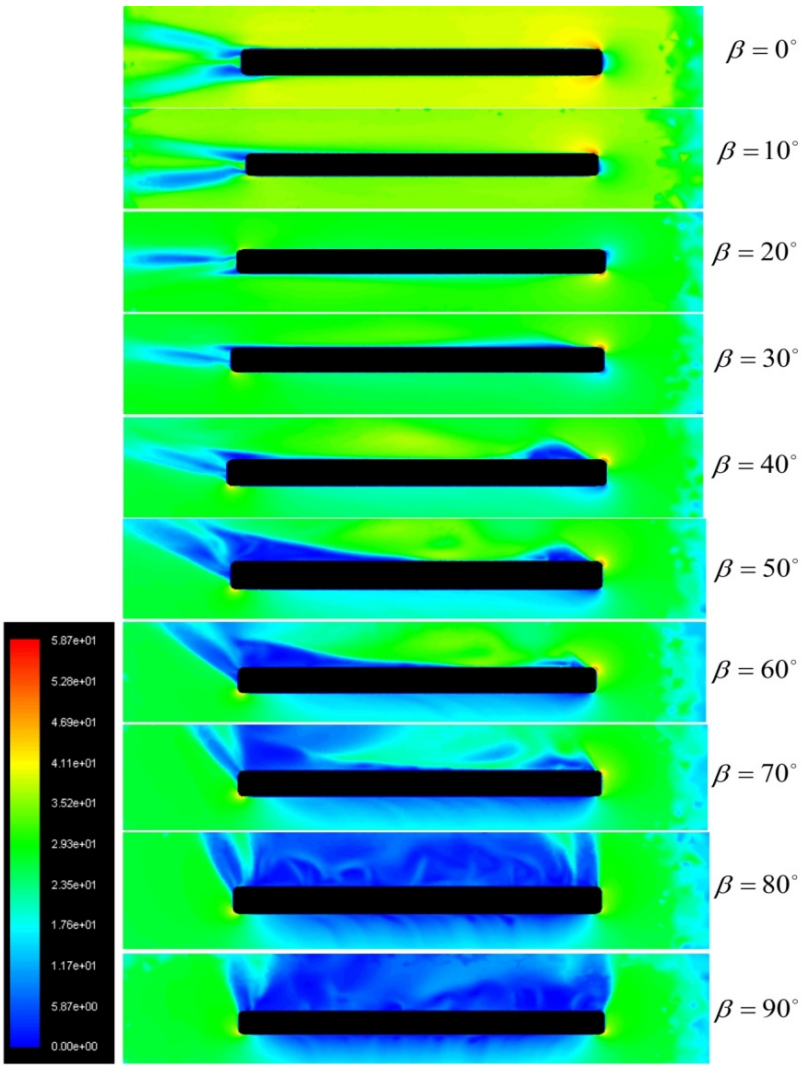


Fig. 9 The top view of the time averaged velocity magnitude at z/ht=0.2 for different yaw angles

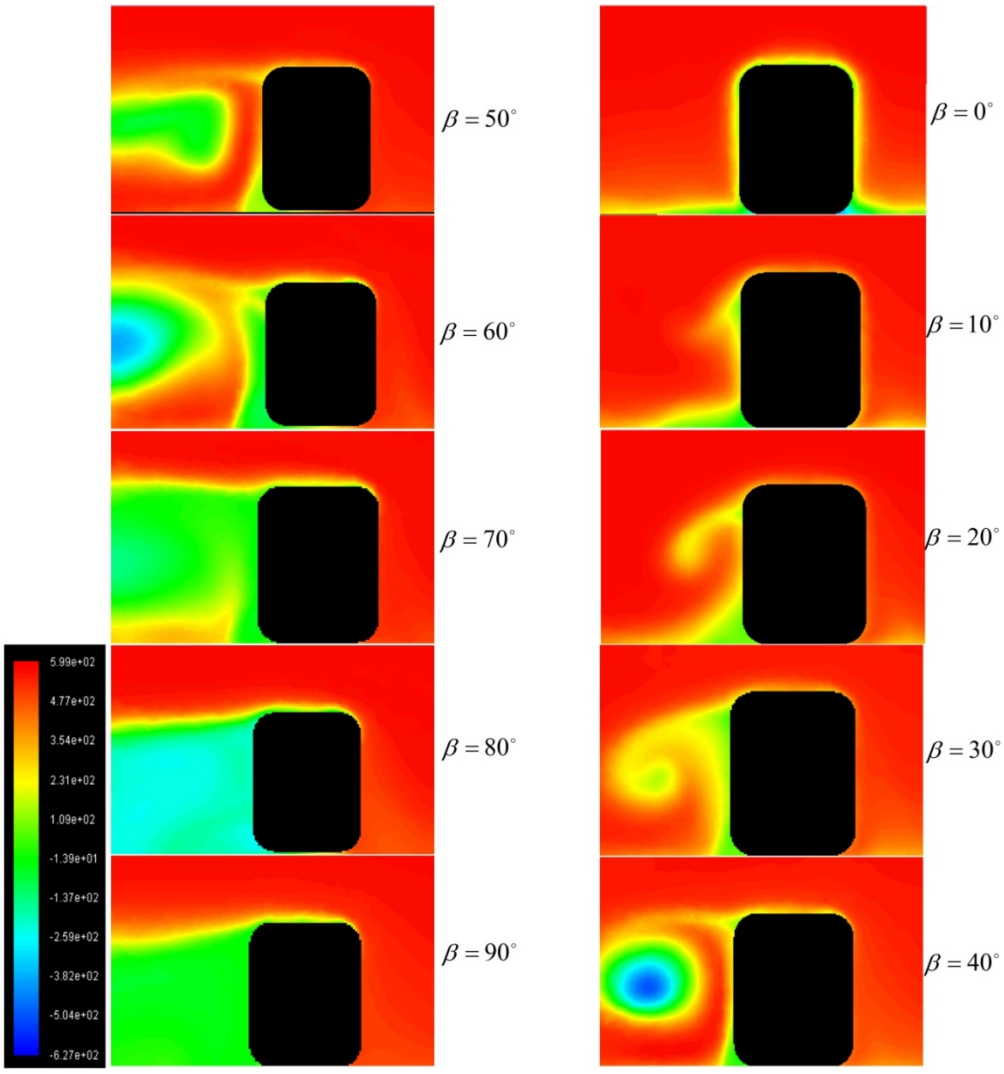


Fig. 10 The total pressure distribution on a section of the train model for yaw angles from 0 to 90 degrees

## 6. Conclusions

This research focused in studying the flow fields around an ATM high speed train. It aimed at summarizing the numerical assessment of the aerodynamic characterization of a high speed train in different crosswinds. The numerical results are compared with the experiment data in order to validate the numerical procedure. The boundary conditions relevant to the subject were selected on the bases that facilitate simulation of the real case scenarios as much as possible. It is to form the turbulent flow and to put the train model under the layer of the logarithmic law that represents the completely developed flow. A sensitivity study of the results with respect to the variations in the angle and speed of wind to the turbulence methods and order of discretization of the convective scheme are made. It is found that the best agreement with experimental results corresponds to the κ-ε realizable turbulence model. The dependency of the flow structure on the different yaw angles studied. Based on the analysis of the results, the following can be reported:

- Drag and side forces coefficients and yawing moment in any yaw angle are almost independent of the flow speed in the whole range of the tested flow speed.
- The vital characteristic wind curve is presented. It is generated by evaluating the train speed limit under various wind conditions before the vehicle runs the risk of overturning. The data on this curve can be used for the processes of aerodynamic optimization of the vehicle. It can also be used for the risk assessment procedures.
- With increase in the yaw angle, the drag and side force and yawing moments are increased.

The originality in this research can be attributed to its' method of solution and the findings of all aerodynamic coefficients and the wind characteristic curves at various speed (i.e. 7-70 m/s) and at various relative wind angles (0-90 degrees). No such global comparison for the specified train was reported. All comparisons reported prior to this research either cover a very limited domain of angles or due to the restricted wind tunnel circumstances could not reach to higher velocity. The method and the type of flow calculations reported in this research are unique and have not been used before, to the extent that is provided.

## Acknowledgments

The Authors of this article would like to acknowledge the support of the research office of Iran University of Science and Technology throughout the course of this study.

## References

Axelsson, N., Ramnefors, M. and Gustafsson, R. (1998), *Accuracy in computational aerodynamics, Part1: Stagnation pressure*SAE 980037.

Baker, C.J. (1991), "Ground vehicles in high cross winds, Part 3: The interaction of aerodynamic forces and the vehicle system", *J. Fluid Struct.*, **5**(2), 221-241.

Baker, C.J., Jones, J., Lopez-Calleja, F. and Munday, J. (2004), "Measurements of the cross wind forces on trains", *J. Wind Eng. Ind. Aerod*., **92**(7-8), 547-563.

Baker, C.J. (2008), "The flow around high speed train", *Proceedings of the BBAA VI International Colloquium on: Bluff Bodies Aerodynamics & Applications*, Milano, Italy, July 20-24.

Cheli, F., Ripamonti, F., Rocchi, D., Tomasini, G. and Zanetti, G. (2006), "Aerodynamic sensitivity analysis

of the new EMUV250 train to cross wind using wind tunnel tests and CFD analysis", *Proceedings of the European Conference on Computational Mechanics Solids, Structures and Coupled Problems in Engineering*, Lisbon, Portugal.

Cheli, F., Ripamonti, F., Rocchi, D. and Tomasini, G. (2010), "Aerodynamic behavior investigation of the new EMUV250 train to cross wind", *J. Wind Eng. Ind. Aerod.*, **98**( 4-5), 189-201.

Cheli, F., Corradi, R. and Tomasini, G. (2012), "Crosswind action on rail vehicles: a methodology for the estimation of the characteristic wind curves", *J. Wind Eng. Ind. Aerod.*, **104-106**, 248-255.

Diedrichs, B. (2003), "On computational fluid dynamics modeling of crosswind effects for high-speed rolling stock", *J. Rail Rapid Transit*, **217**(3), 203-226.

Diedrichs, B. (2005), *Computational methods for crosswind stability of railway trains - a literature survey*, *TRITA-AVE Report*, **27**, ISSN 1651-7660.

Diedrichs, B. (2009), "Unsteady aerodynamic crosswind stability of a high-speed train subjected to gusts of various rates", *Proceedings of the EUROMECH Colloquium 509 Vehicle Aerodynamics - External aerodynamics of railway vehicles, trucks, buses and cars,* Berlin, Germany, March 24-25.

Gawthrope, R.G. (1994), "Wind effects on ground transportation", *J. Wind Eng. Ind. Aerod.*, **52**, 73-92.

Hemida, H., Kraajnvic, S. and Davidson, L. (2005), "Large Eddy simulations of flow around a simplified high-speed train under the influence of a crosswind", *Proceedings of the 17th AIAA Computational Dynamics Conference*, Toronto, Ontario, Canada.

Hemida, H. and Kraajnvic, S. (2006), "Exploring the flow around a generic high-speed train under the influence of side winds using LES", *Proceedings of the CWE2006*, Yokohama, Japan, July.

Hemida, H. and Baker, C.J. (2010), "Large-Eddy simulation of the flow around a freight wagon subjected to a crosswind", *Comput. Fluids*, **39**(10), 1944-1956.

Kandasamy, S., Cheng, H., Lietz, R. and Mallick, S. (2002), *Exterior airflow simulations using a lattice Boltzmann approach*, SAE, 2002-01-0596.

Khier, W., Breuer, M. and Durst, F, (2000), "Flow structure around trains under side wind conditions: a numerical study", *Comput.Fluids*, **29**(2), 179-195.

Masbernat, F., Wolffhugel, Y.F. and Dumas, J.C. (1993), *CFD Aerodynamics of the French high-speed train*, GEC ALSTHOM Technical Review, No. 11.

Masson, E., Allain, E. and Parardot, N. (2009), "CFD Analysis of the underfloor aerodynamic of a complete TGV high speed trainset at full scale", *Proceedings of the EUROMECH Colloquium 509 Vehicle Aerodynamics - External Aerodynamics of Railway Vehicles, Trucks, Buses and Cars*, Berlin, Germany, March 24-25.

prEN 14067-6. Railway Applications – Aerodynamics – Part 6: Requirements and test procedures for cross wind assessment, *European Standard.*

Rocchi, D., Schober, M., Cheli, F., Orellano, A. and Tomasini, G. (2009), "Comparison of wind tunnel tests results on the ATM train", *Proceedings of the Euromech Colloqium 509, Vehicle Aerodynamics*, Berlin, Germany, March 24-25.

Rolen, C., Rung, T. and Wu, D. (2004), "Computational modeling of crosswind stability of high speed trains", *Proceedings of the European Congress on Computational Methods in Applied Sciences and Engineering, ECCOMAS 2004*, July 24-28.

Sharma, R., Chadwick, D. and Haines, J. (2008), "Aerodynamic of an intercity bus", *Wind Struct.*, **11**(4), 257-273.

Simulation software (2012), *Student edition of ANSYS Fluent CFD software*, ANSYS Inc.

Suzuki, M., Tanemoto, K. and Maeda, T. (2003), "Aerodynamic characteristics of train/vehicles under cross winds", *J. Wind Eng. Ind. Aerod.*, **91**(1-2), 209-218.

Versteeg, H.K. and Malalasekera, W. (2007), *An introduction to computational fluid dynamics - the finite volume method*, Pearson Education Limited, 2nd Ed.

White, F.M. (2008), *Fluid mechanics*, 6th Ed., McGraw-Hill, New York.

Xu, Y.L. and Guo, W.H. (2003), "Dynamic behavior of high-sided road vehicles subject to a sudden crosswind gust", *Wind Struct.*, **6**(5), 325-346.

Yang, Z.G., Johnson, J.P., Morley, J.B., Unaune, S. and Sovani, S.D. (2007), *Dynamic moving mesh CFD*

*study of semi-truck passing a stationary vehicle with hood open*, *Vehicle Aerodynamics*, SAE paper 2007-01-0111.
Yau, J.D. (2012), "Lateral vibration control of a low-speed maglev vehicle in cross winds", *Wind Struct.*, **15**(3), 263-283.

*CC*

## Nomenclature

| | | | |
|---|---|---|---|
| $A_t$ | Projected area | $u^+$ | Dimensionless mean velocity |
| $C_i$ | Force coefficient | $v$ | y-component of velocity |
| $C_j$ | Moment coefficient | $\overline{v}$ | Time averaged y-component of velocity |
| $F_i$ | Force | $v'$ | Fluctuating y-component of velocity |
| $M_j$ | Moment | $w$ | z-component of velocity |
| $q$ | Dynamic head pressure | $\overline{w}$ | Time averaged z-component of velocity |
| $C_p$ | Pressure coefficient | $w'$ | Fluctuating z-component of velocity |
| $\rho$ | density | $y^+$ | Dimensionless wall distance |
| $k$ | Kinetic energy | $\beta$ | Yaw angle |
| $l_t$ | Characteristic length | $\varepsilon$ | Dissipation of kinetic energy |
| $Ma$ | Mach number | $\omega$ | Frequency of kinetic energy |
| $p$ | Pressure | $M_{Grav}$ | Moment of gravity |
| $\overline{p}$ | Time averaged component of pressure | $M_{aero}$ | Moment of aerodynamic |
| $p'$ | Fluctuating component of pressure | $m$ | Mass of train |
| Re | Reynolds number | $g$ | Gravity constant |
| $U_\infty$ | Free stream velocity | $U_R$ | Relative velocity |
| $u$ | x-component of velocity | $U_t$ | Train velocity |
| $\overline{u}$ | Time averaged x-component of velocity | $U_w$ | Wind velocity |
| $u'$ | Fluctuating x-component of velocity | $h_t$ | Train height |

## Abbreviations

| | |
|---|---|
| ATM | Aerodynamic Train Model |
| CFD | Computational Fluid Dynamics |
| RANS | Reynolds-Averaged Navier-Stokes |
| LES | Large Eddy Simulation |
| DNS | Direct Numerical Simulation |
| LBM | Lattice Boltzmann Method |